

AD-A081 656

MCDONNELL DOUGLAS ASTRONAUTICS CO ST LOUIS MO
LASER COMMUNICATION CLIMATOLOGY STUDY. (U)
MAY 79

F/6 17/2

N00014-78-C-0539

UNCLASSIFIED

NL

1 of 1
AD
A081656

END
DATE
FILMED
4-80
DPC

ADA 081 656

11/25 MAY 1979

12 23

APPROVED FOR PUBLIC RELEASE
DISTRIBUTION

DTIC ELECTE
MAR 5 1980
S D
B
1

6 LASER COMMUNICATION CLIMATOLOGY STUDY.

9 INTERIM REPORT.

CONTRACT 15 N00014-78-C-0539

This report summarizes the progress made during the first half of the climatology study contract period. It presents preliminary results which are useful in estimating the availability of space-to-earth optical communication systems.

DISTRIBUTION STATEMENT A
Approved for public release;
Distribution Unlimited

LEVEL II

I. Review of 3DNEPH Data Base

This study uses MDAC software which was especially designed to infer the statistics of cloud optical and physical thickness for any location using the Air Force 3DNEPH Global Cloud Data Base. The 3DNEPH data is produced once every 3 hours from January 1972 to present for a grid of points covering the entire world. Figure 1 shows the 3DNEPH sampling grid for the Northern Hemisphere. The hemisphere is divided into 64 boxes, each of which in turn is divided into a matrix of 64 rows and 64 columns. The distance between these grid points is approximately 25 nautical miles, which provides good horizontal resolution. Each 3DNEPH data record contains 22 parameters which are used in the MDAC software to compute the cloud thickness statistics. The parameters are: types of low, middle and high clouds, present weather, maximum cloud top and minimum cloud base altitudes, total cloud cover, and percent cloud coverage in each of 15 nonuniform thickness layers extending from sea level to a maximum of 55,000 feet above sea level. Figure 2 shows a sample 3DNEPH record for Malta and Figure 3 illustrates the arrangement of the 15 layers along with the types of low, middle, and high clouds reported.

THE RUTH H. HOOKER
TECHNICAL LIBRARY

JUN 07 1979

JUL 19 1979

II. MDAC 3DNEPH Processor

Figure 4 shows a simplified flow diagram of the MDAC 3DNEPH processor. The Processor scans each 3DNEPH data sample given using the layered cloud coverage along with the maximum cloud top and minimum cloud base altitudes to compute a characteristic optical thickness for low, middle and high clouds. Statistical independence between these three cloud bands is then assumed and the probabilities of one or more simultaneous occurrence of these optical thicknesses are then computed. This results in up to eight optical thickness samples for each 3DNEPH data sample. The processor has been updated to output physical thickness as well as optical thickness. By using the physical thickness associated with each

NAVAL RESEARCH LABORATORY

McDONNELL DOUGLAS AERONAUTICS COMPANY 404251
ST. LOUIS MISSOURI 63166

Figure 1

3DNEPH BOXES

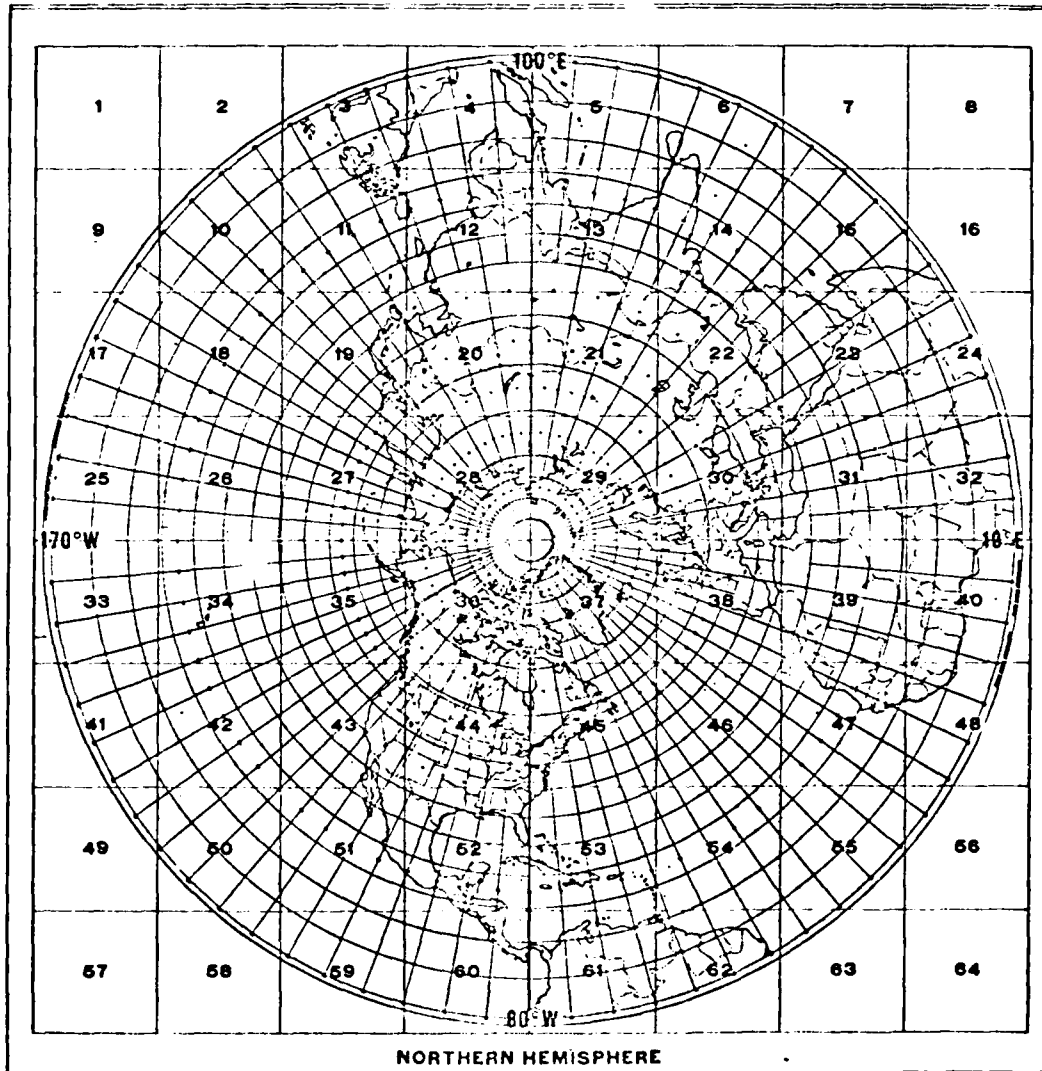
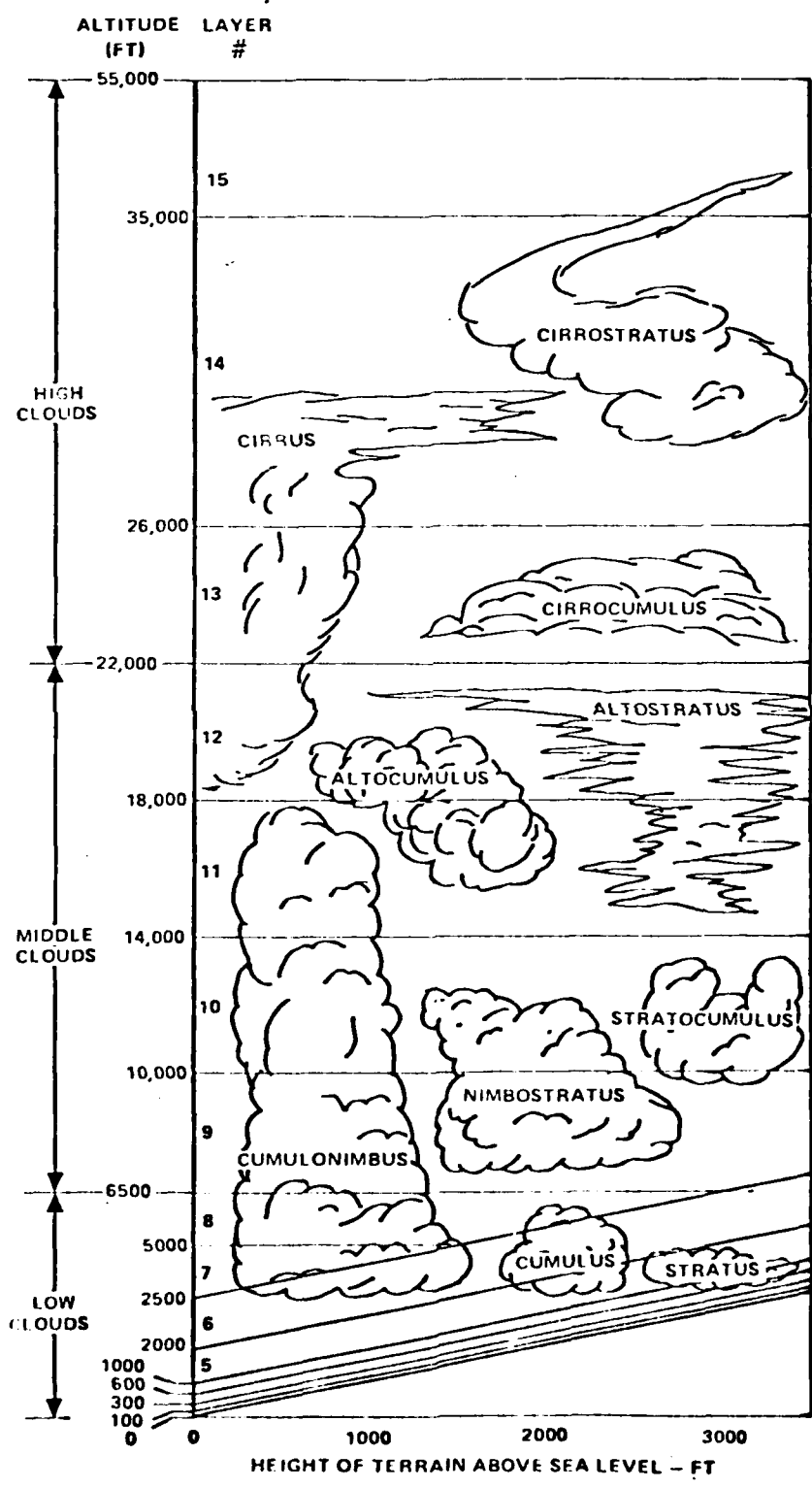


Figure 3

3D NEPH CLOUD DEFINITION



MDAC 3DNEPH PROCESSOR SIMPLIFIED FLOW DIAGRAM

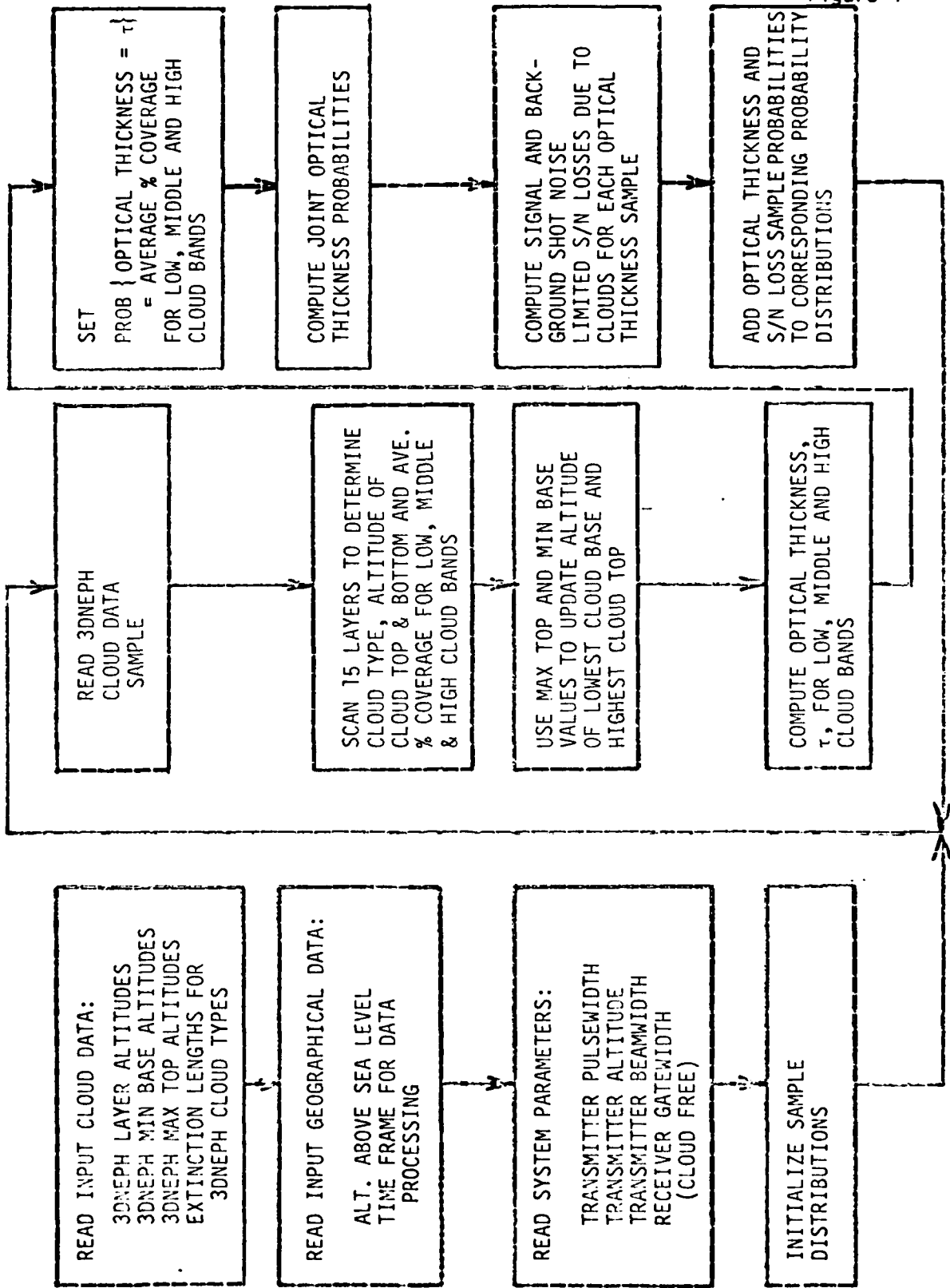


Figure 4

optical thickness sample a joint statistical distribution of optical and physical thickness is obtained.

The MDAC 3DNEPH processor has been verified by comparing the yearly optical thickness distributions it outputs with those inferred from independently produced solar transmission data for several locations. Figures 5 and 6 show sample comparisons for Malta and St. Louis, respectively. Cloud optical thickness is inferred from solar transmission by using the Bucher cloud transmission model ⁽¹⁾ which we have verified by computer simulation. ⁽²⁾

III. Laser Climatology Preliminary Results

One of the first questions addressed in the study is the duration of time over which the 3DNEPH data must be processed in order to obtain a meaningful representation of cloud statistics for the ocean areas. Figure 6 shows a comparison of the 3DNEPH optical thickness distribution for the years 1972 thru 1976 with that for 1972 alone for a location in the Central Pacific. Note that the difference between the two distributions is only a few percent. The same is true for a location in the Atlantic, as shown in Figure 7. The conclusion is that one year is representative enough to give estimates of availability accurate to within a few percent. The next question is the extent to which averaging over the mid-season months is representative of averaging over the entire year. Figure 8 shows a comparison of optical thickness distributions for both the midseason months and the entire year of 1972 at locations in the Pacific and Atlantic. Note that the midseason months indicate cloud thickness statistics which are within a few percent of those for the entire year. We thus anticipate that processing the 3DNEPH cloud data over the midseason months of a single year (1972) for all locations in this study will allow the OPSATCOM system availability to be estimated to within a few percent.

In addition to investigating the yearly distribution of optical thickness, we also looked at the distributions on a monthly basis. Figure 9 shows optical thickness distributions for the midseason months of January, April, July, and October, 1972 for Atlantic City, N. J. As expected, the clouds are thickest in the month

Figure 5

OPTICAL THICKNESS DISTRIBUTION FUNCTIONS FOR MALTA:
COMPARISON OF GLOBAL RADIATION AND 3D NEPH DATA

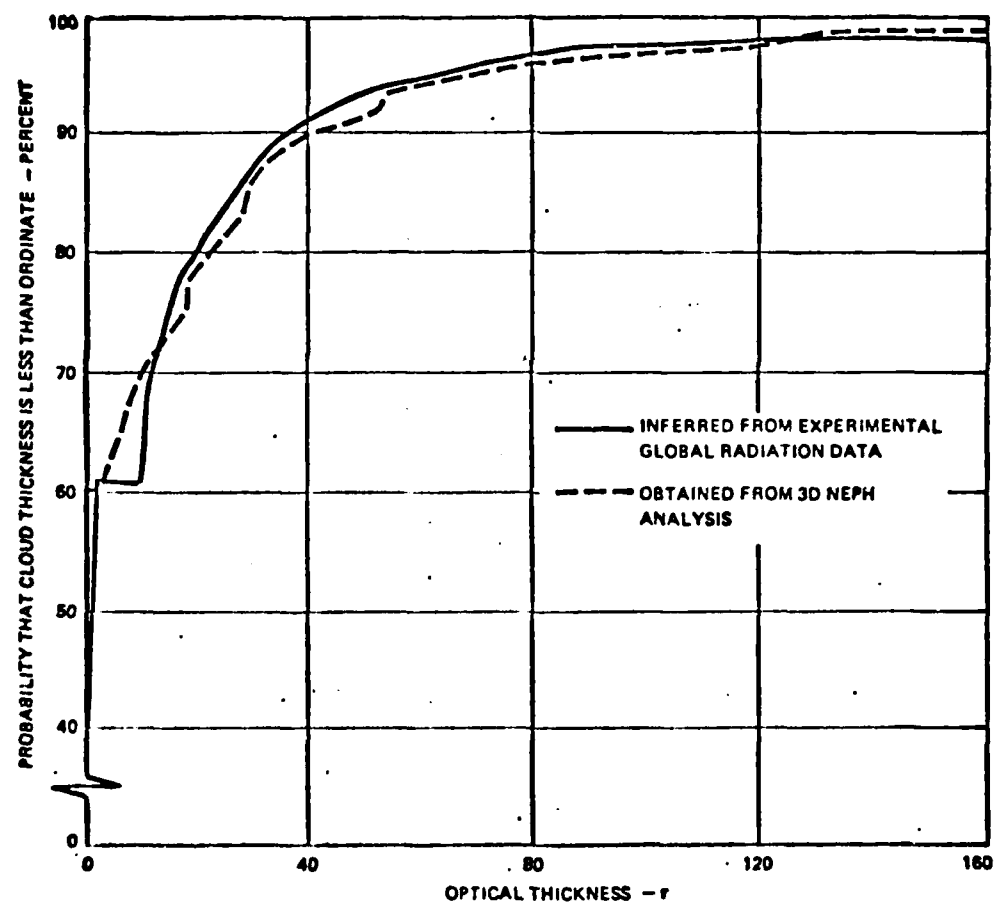


Figure 6

COMPARISON OF OPTICAL THICKNESS DISTRIBUTIONS FOR ST. LOUIS, 1976

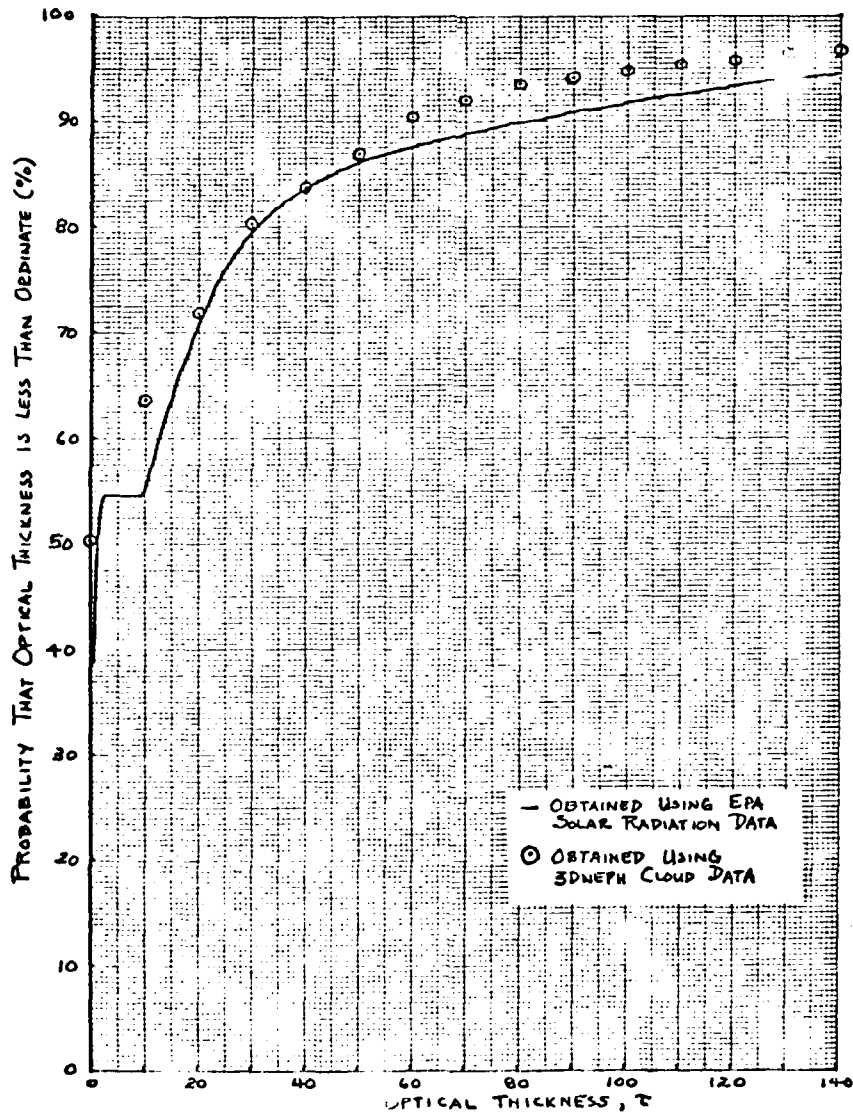


Figure 7

COMPARISON OF OPTICAL THICKNESS DISTRIBUTIONS FOR
CENTRAL PACIFIC, (LAT, LON)=(34°N, 164°E)

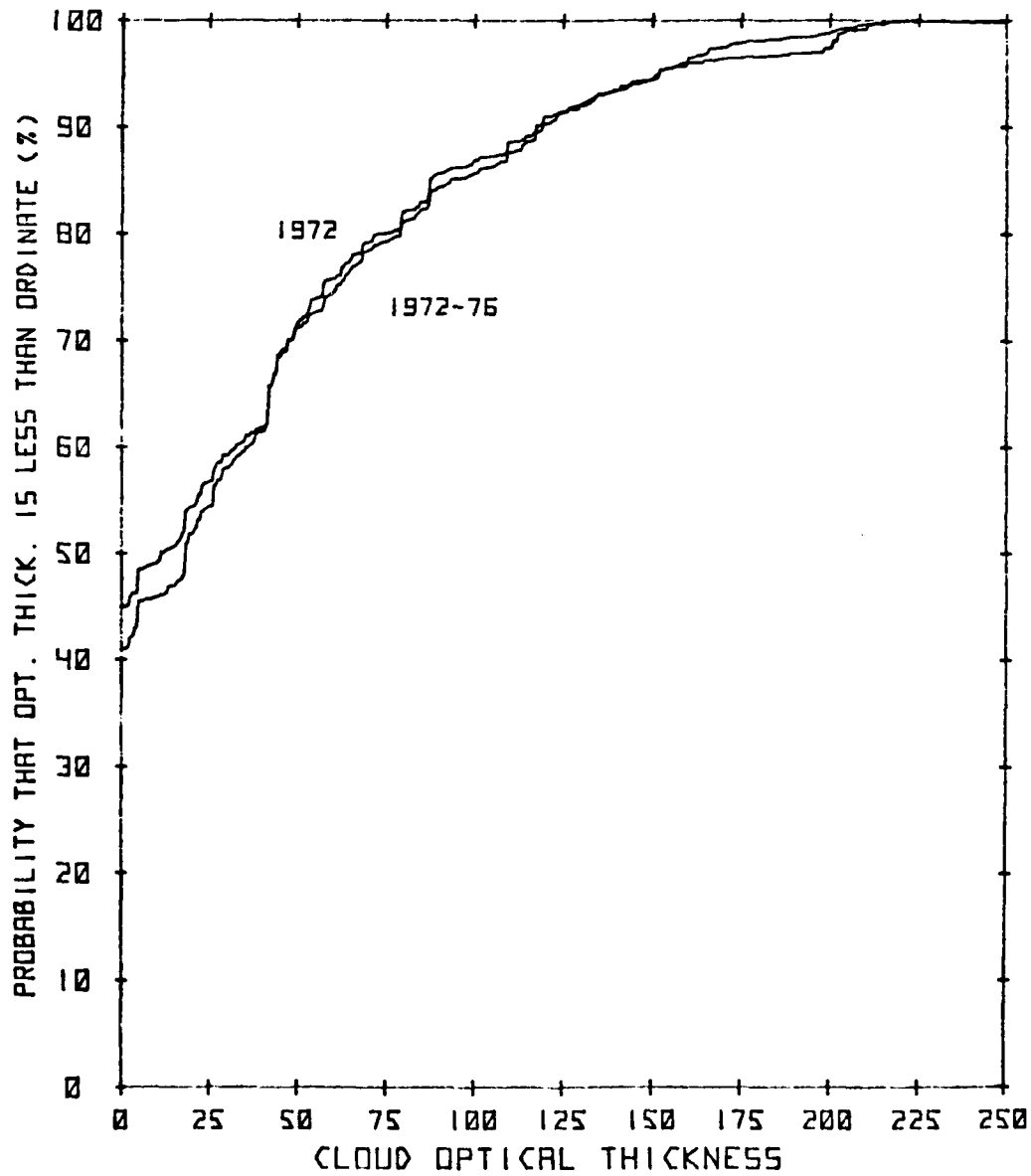
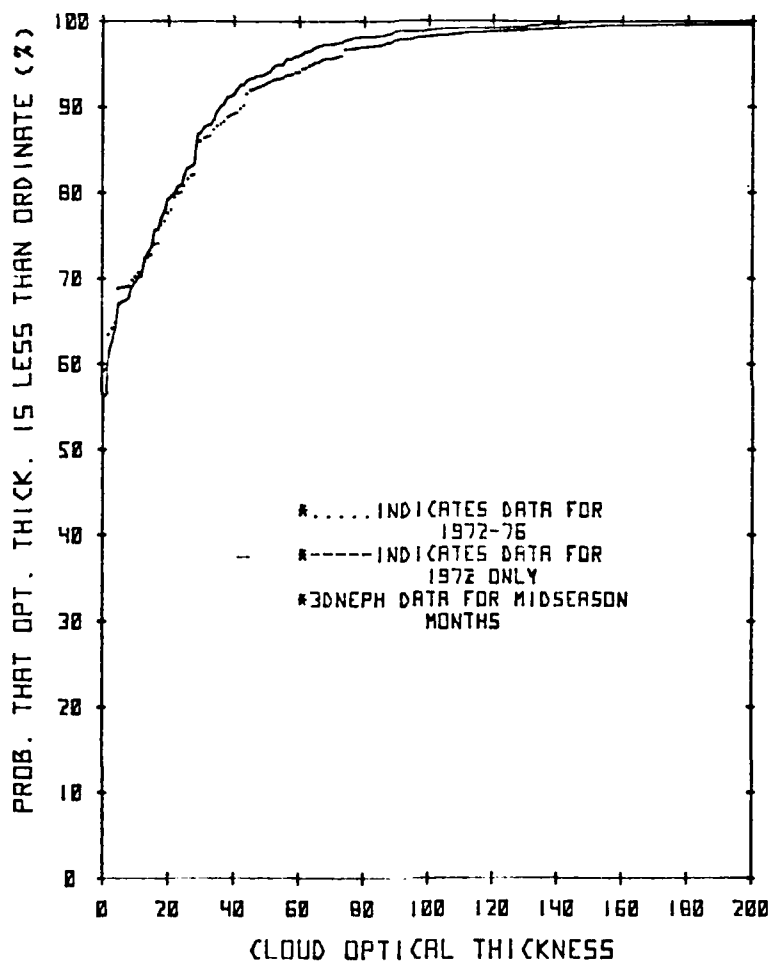
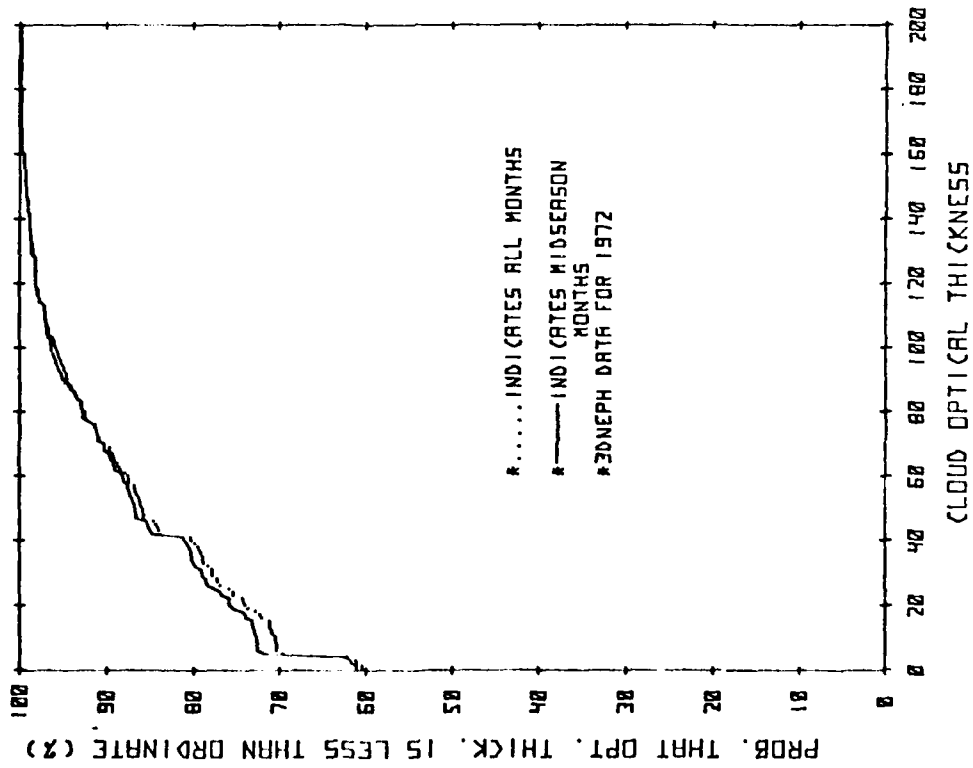


Figure 8

COMPARISON OF OPTICAL THICK. DIST.
TAKEN OVER ONE AND FIVE YEARS
FOR LOCATION IN ATLANTIC
(LAT, LONG) = (40°N, 0°W)



COMPARISON OF MIDSEASON AND FULL
YEARLY OPT. THICK. DIST. FOR
LOCATION IN PACIFIC
(LAT/LONG) = (20°N, 105°W)



COMPARISON OF MIDSEASON AND FULL
YEARLY OPT. THICK. DIST. FOR
LOCATION IN ATLANTIC
(LAT/LONG) = (40°N, 0°W)

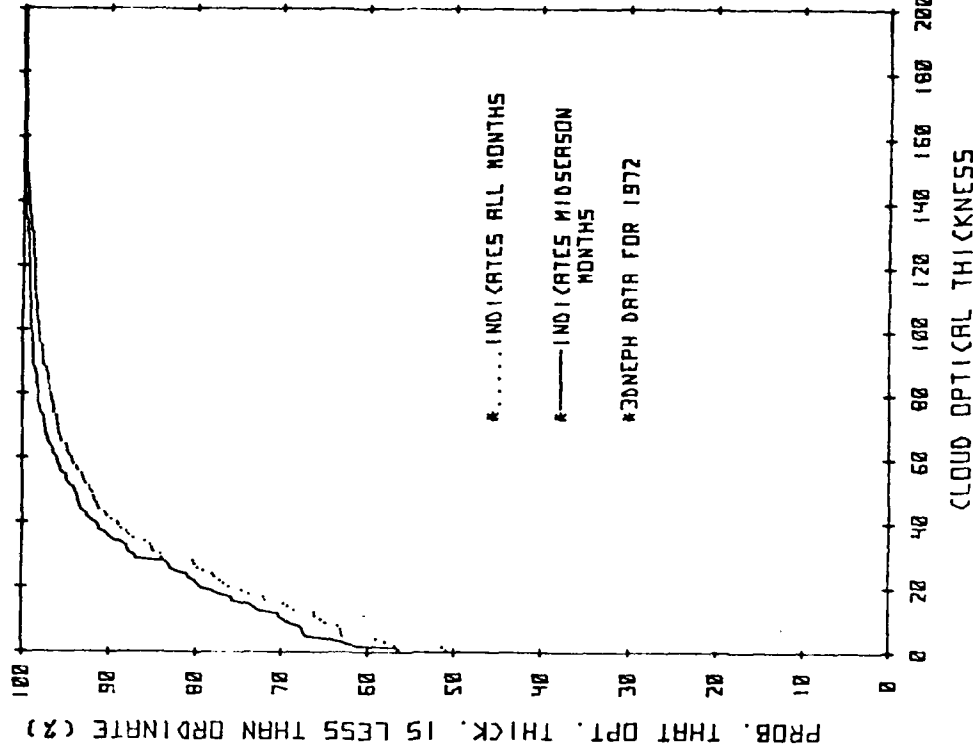
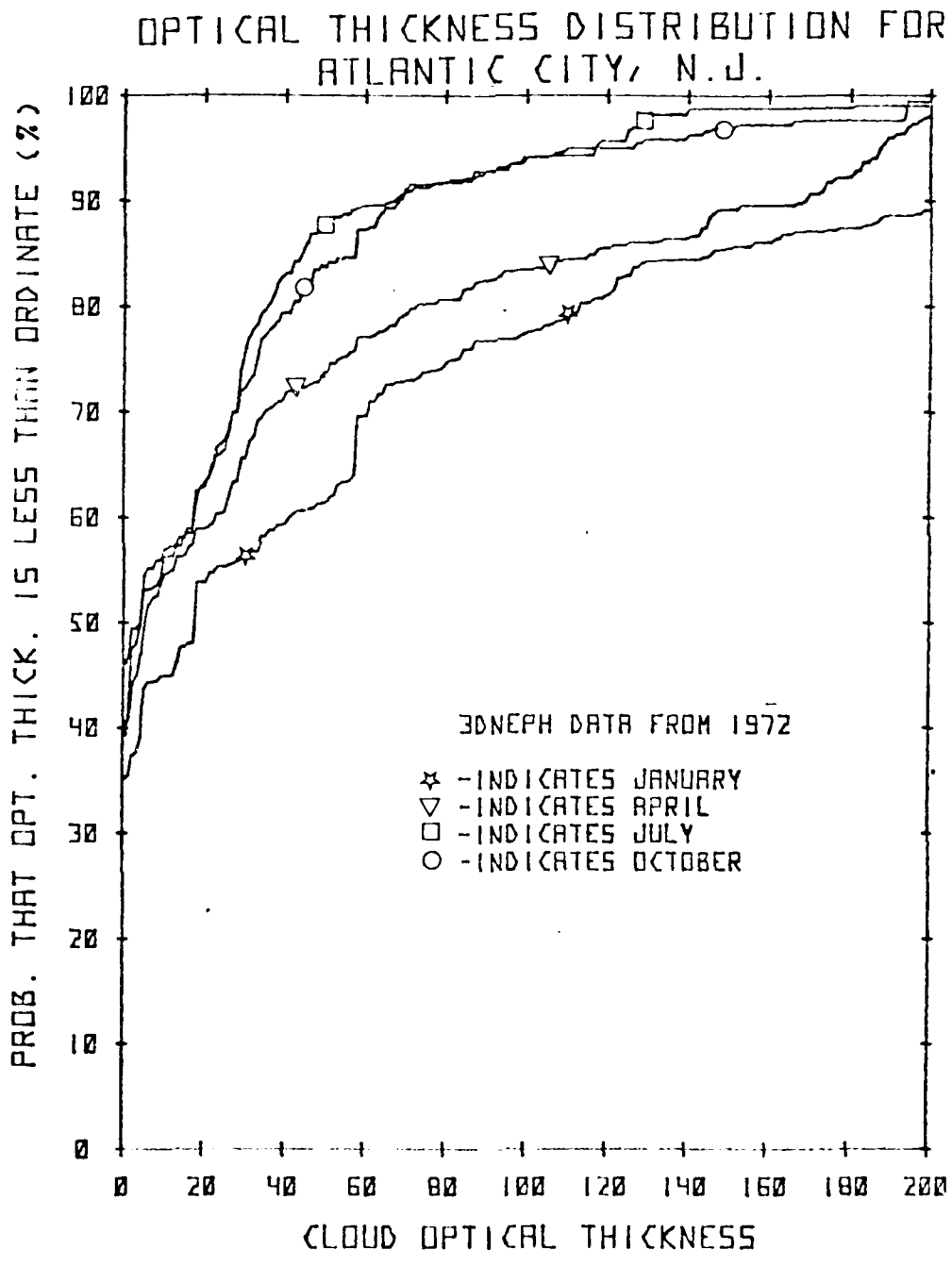


Figure 9

Figure 10



of January and thinnest in the month of July. Given the variability in cloud thickness from season to season as shown in Figure 10, it may be more desirable to include the distributions for the midseason months for each location in addition to the yearly distributions.

After processing some forty locations for the study thus far, several interesting observations were made. First, the high degree of variability in cloud conditions from Central Pacific ocean sites to North Atlantic ocean sites is illustrated in Figure 11, a plot of physical thickness distributions. It shows that there is a 50 percent difference in probability of cloud-free line-of-sight, PCFLOS, (i.e., probability of zero thickness) and that thick clouds occur much more frequently in the North Atlantic than in the Central Pacific. For example, note from Figure 11 that clouds thicker than 5km occur 15 percent of the year in the North Atlantic but only 2 percent of the year in the Central Pacific for the sites shown. The corresponding optical thickness distributions for these locations are shown in Figure 12. Note that in order to achieve 90 percent availability in the Central Pacific a system must be able to penetrate clouds up to an optical thickness of 50, whereas a system in the North Atlantic must penetrate clouds of optical thickness 145 to achieve the same availability. This represents a difference in cloud transmission loss on the order of 4dB and a difference in pulse stretching of about 12dB. Under background shot noise limited operating conditions, this represents a difference of 8dB in required signal power.

Another observation made after processing the data was that cloud conditions are constant over significant changes in longitude but fairly sensitive to latitude for some locations in the Pacific and Atlantic. For example, Figure 13 shows the 3DNEPH optical thickness distributions for two locations in the Pacific, both at 30° N latitude but separated by 30° in longitude. Note the similarity in the distributions. The distributions for two locations at the same longitudes but at an additional 10° in northerly latitude are shown in Figure 14. The cloud conditions again are somewhat constant with longitude but the increase in latitude

Figure 11

COMPARISON OF BEST-CASE AND WORST-CASE
PHYSICAL THICKNESS DISTRIBUTIONS

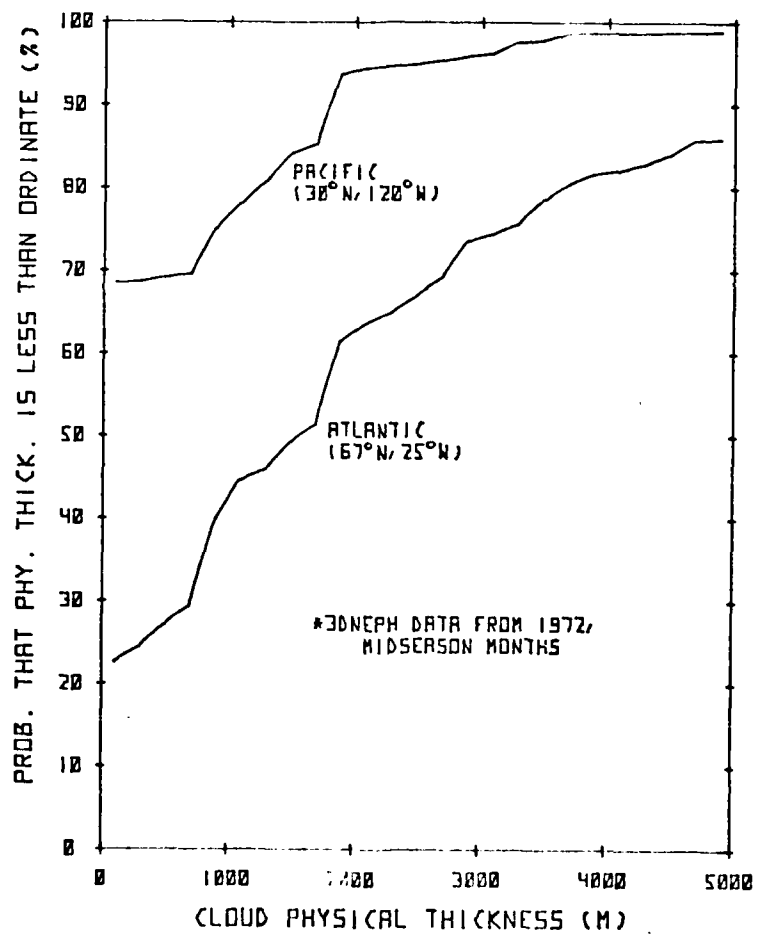


Figure 12

COMPARISON OF BEST-CASE AND WORST-CASE OPTICAL THICKNESS DISTRIBUTIONS

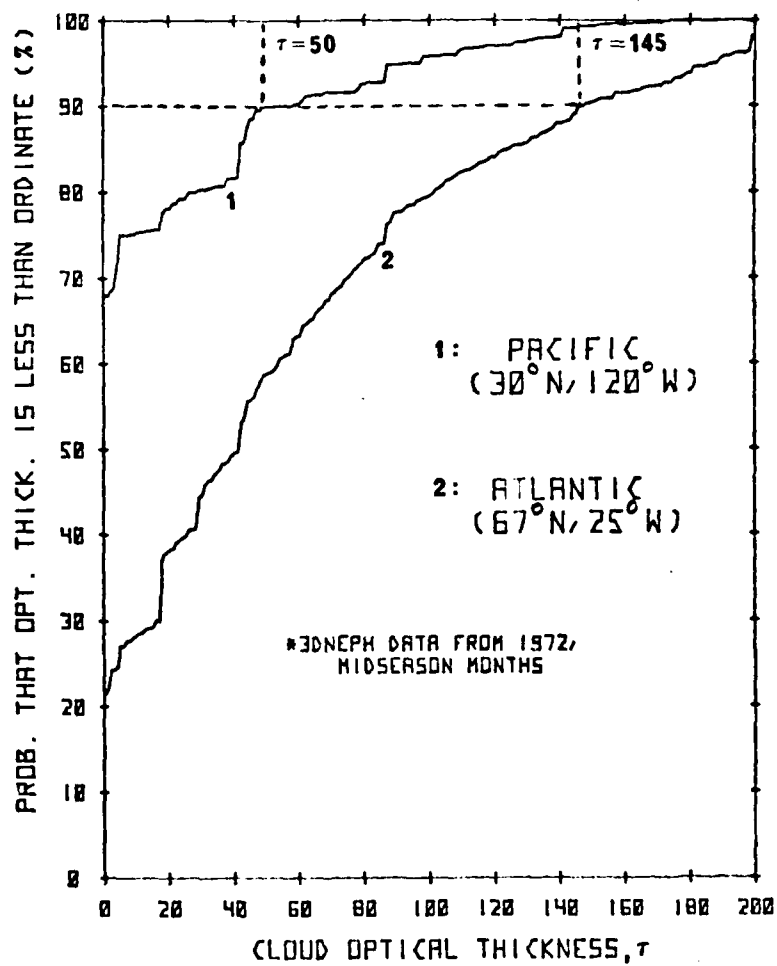


Figure 13

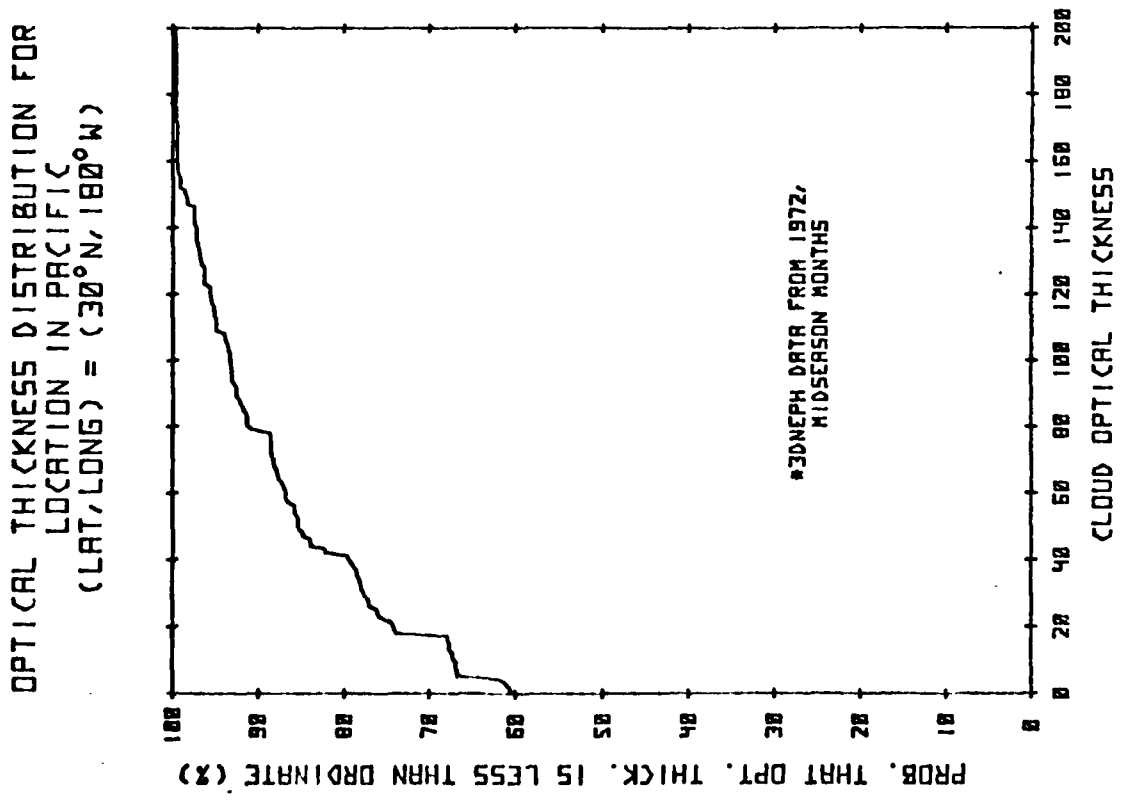
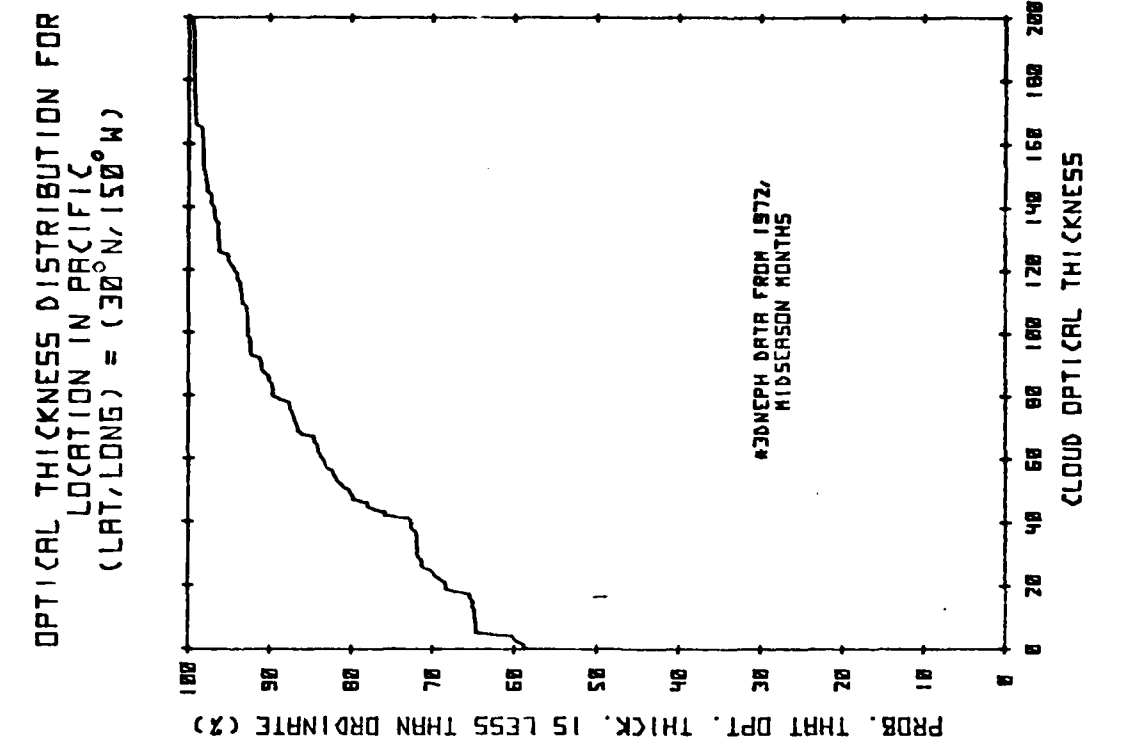
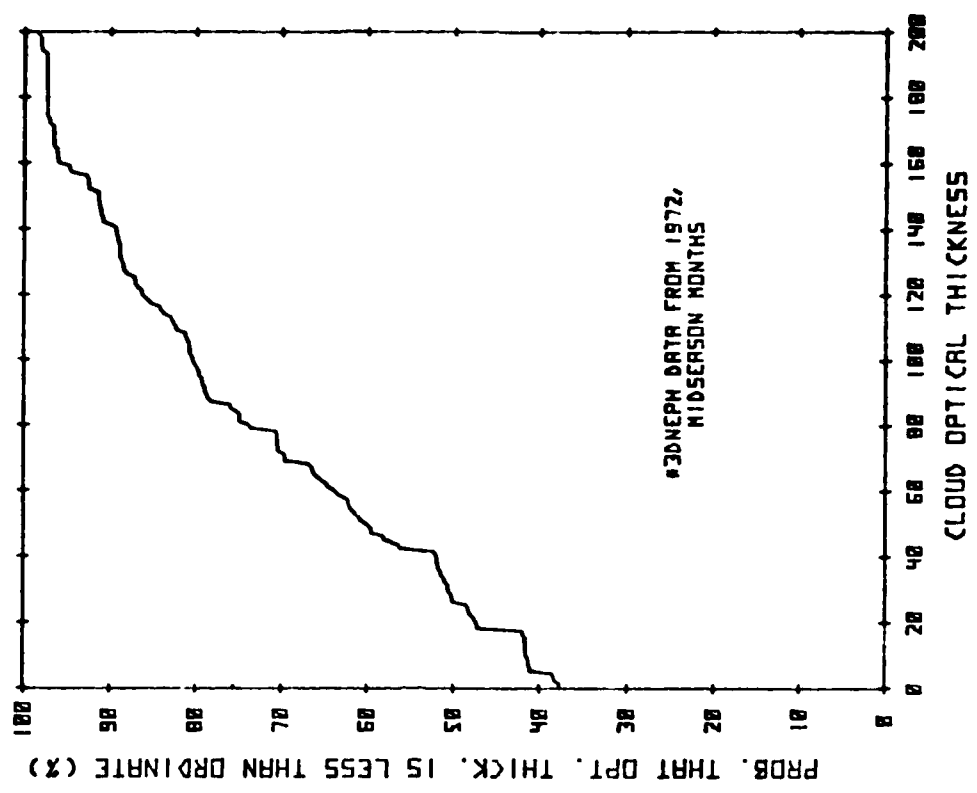
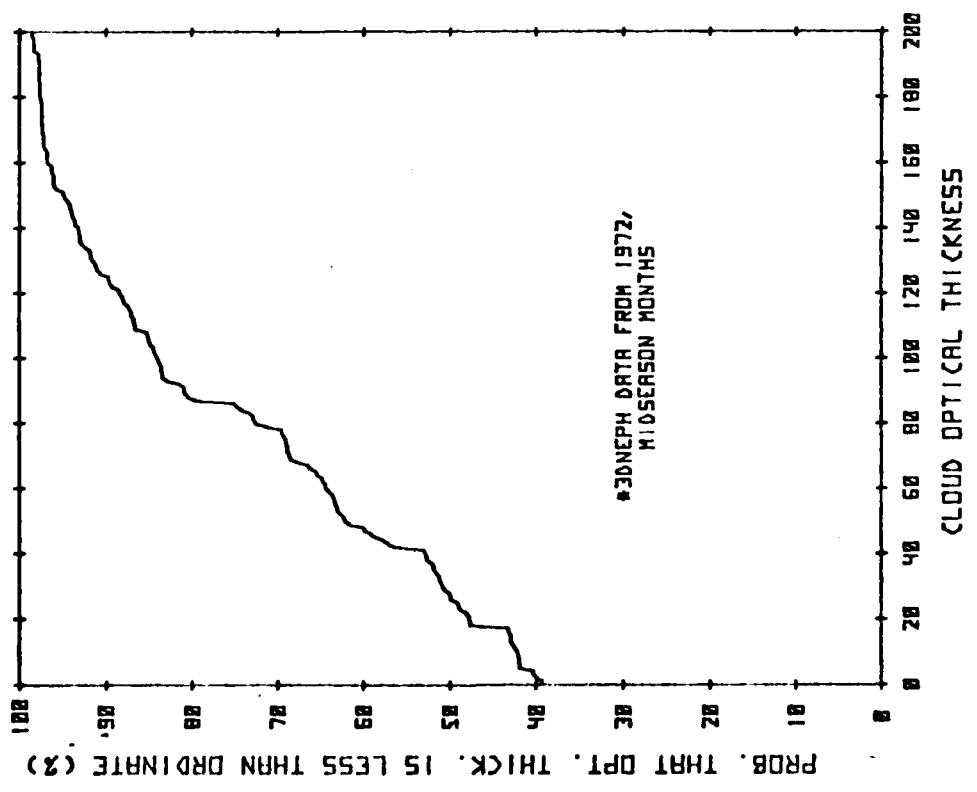


Figure 14

OPTICAL THICKNESS DISTRIBUTION FOR
LOCATION IN PACIFIC
(LAT, LONG) = (40°N, 150°W)



OPTICAL THICKNESS DISTRIBUTION FOR
LOCATION IN PACIFIC
(LAT, LONG) = (40°N, 180°W)



has resulted in both a lower PCFLOS and thicker clouds. These same characteristics appear with an additional increase of 10° in northerly latitude, as shown in Figure 15. Figures 16 and 17 show the same effects in the Atlantic. However, the correlation distance in longitude (15°) is smaller than that noted for the Pacific (30°).

Finally, Figure 18 shows a third order least squares polynomial curve fit to an optical thickness distribution in the Pacific. Such a curve fit is useful for representing the cloud statistics in OPSATCOM system design studies and simulations. The fit is analytically represented by

$$\tau = \begin{cases} \sum_{i=0}^N a_i f^i & , f_0 < f \leq 1 \\ 0 & , 0 \leq f \leq f_0 \end{cases} \quad (1)$$

where

f = Probability { optical thickness $\leq \tau$ }

f_0 = Probability { optical thickness = 0 }

a_i = Least squares coefficients

N = Order of fit ($N = 3$ in Figure 18)

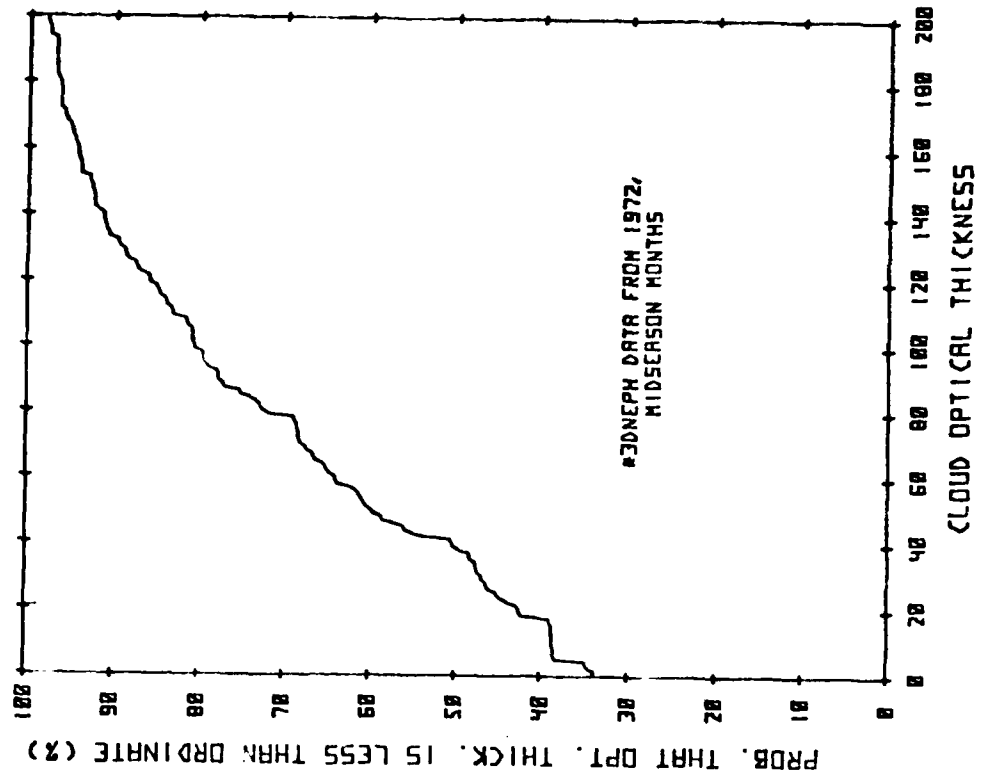
In a Monte Carlo simulation, f would be a random number uniformly distributed between 0 and 1, and the corresponding optical thickness would be computed using f in equation (1). In this manner, random optical thickness samples would be drawn from a distribution which approximates the 3DNEPH distribution to within a few percent, as shown in Figure 18. The values of a_i , f_0 and N vs. location are shown in Figure 19.

References

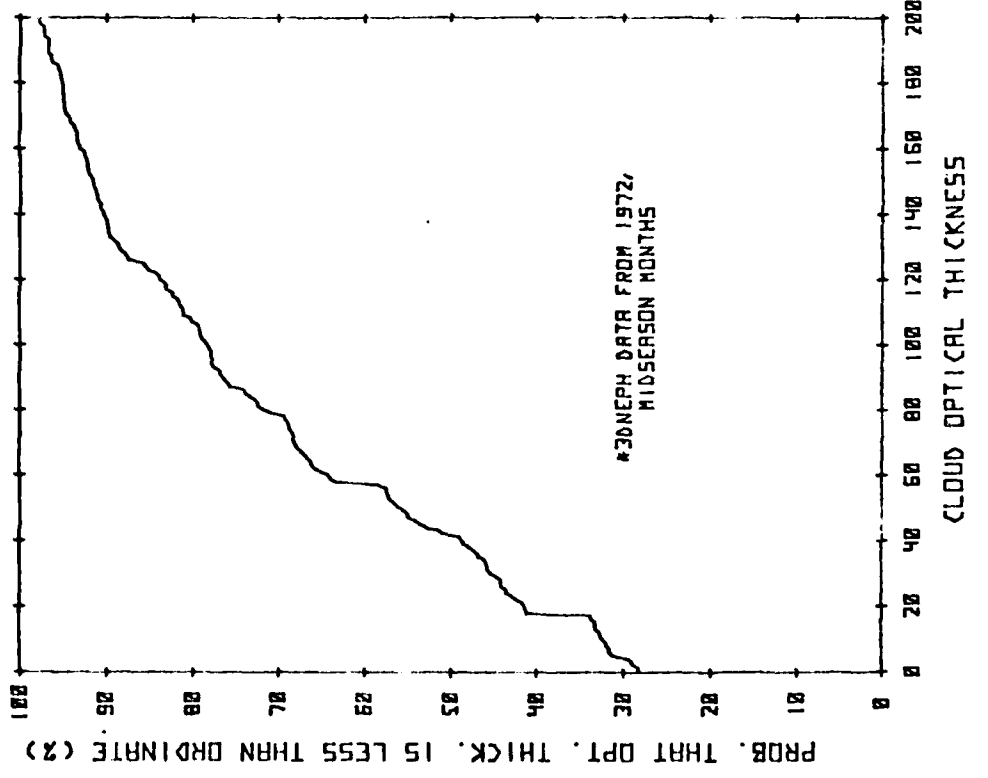
1. E. A. Bucher, "Computer Simulation of Light Pulse Propagation for Communication through Thick Clouds," Applied Optics, Vol. 12, #10, Oct. 1973.
2. G. Lee, C. Cianny, G. Schroeder, J. Fenier, "Availability Models for Space-to-Earth Optical Communication Links," to be published.

Figure 15

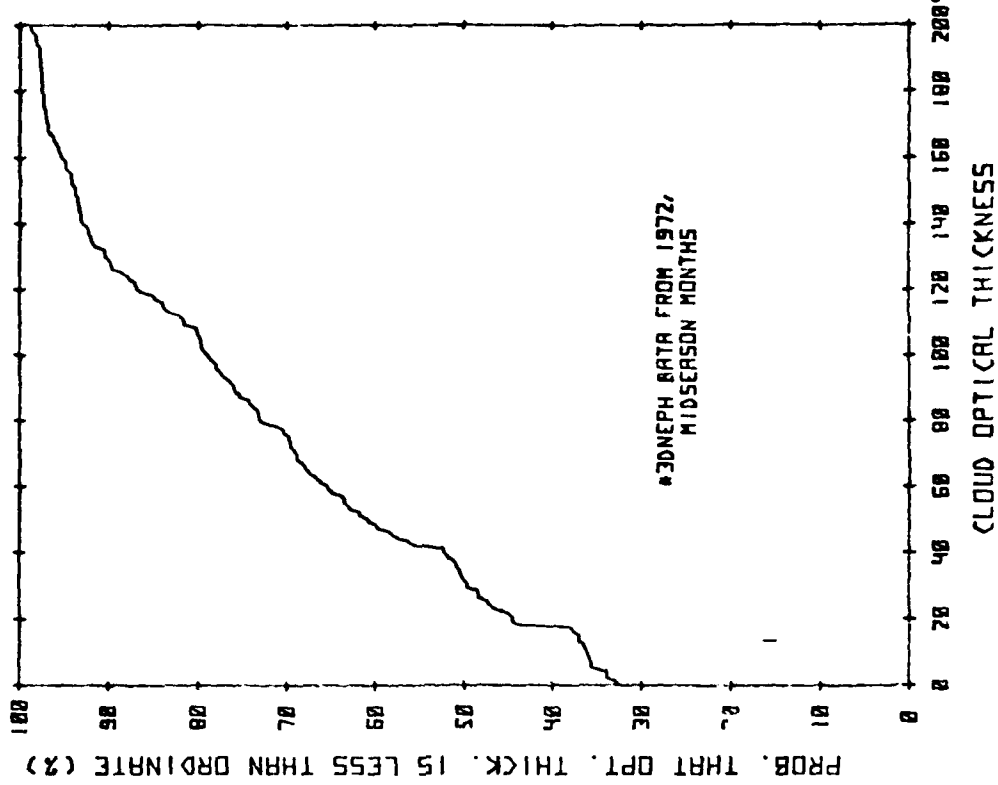
OPTICAL THICKNESS DISTRIBUTION FOR
LOCATION IN PACIFIC
(LAT, LONG) = (50°N, 150°W)



OPTICAL THICKNESS DISTRIBUTION FOR
LOCATION IN PACIFIC,
(LAT, LONG) = (50°N, 180°E)



OPTICAL THICKNESS DISTRIBUTION FOR
LOCATION IN ATLANTIC
(LAT, LONG) = (50°N, 15°W)



OPTICAL THICKNESS DISTRIBUTION FOR
LOCATION IN ATLANTIC
(LAT, LONG) = (50°N, 30°W)

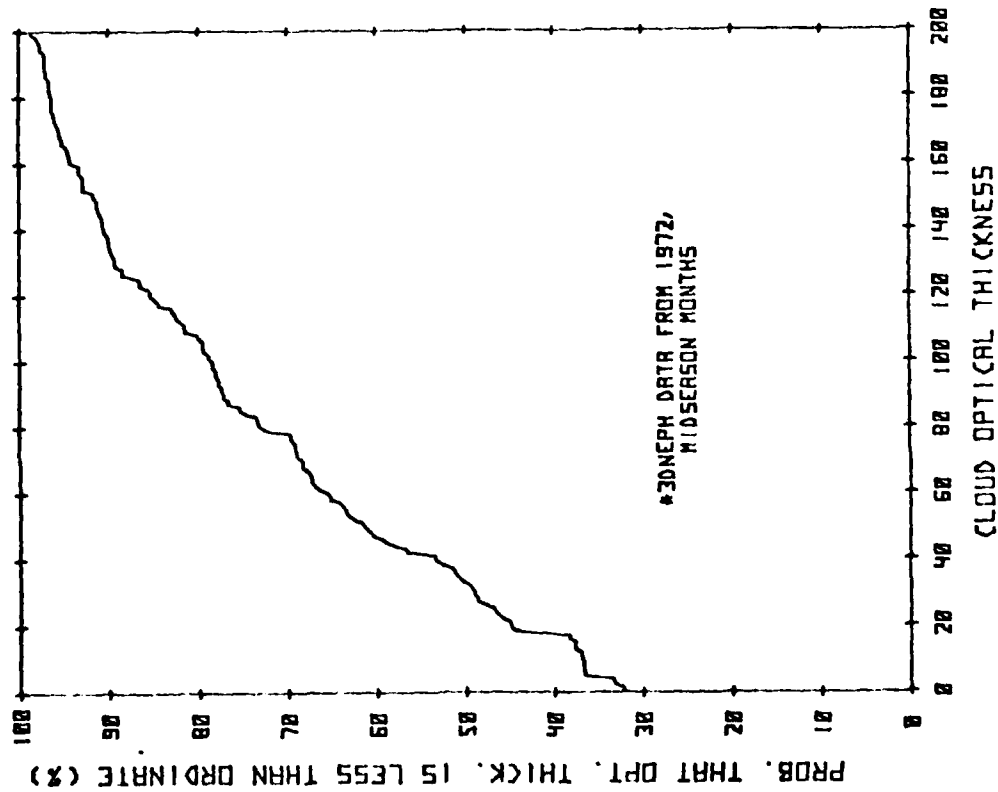
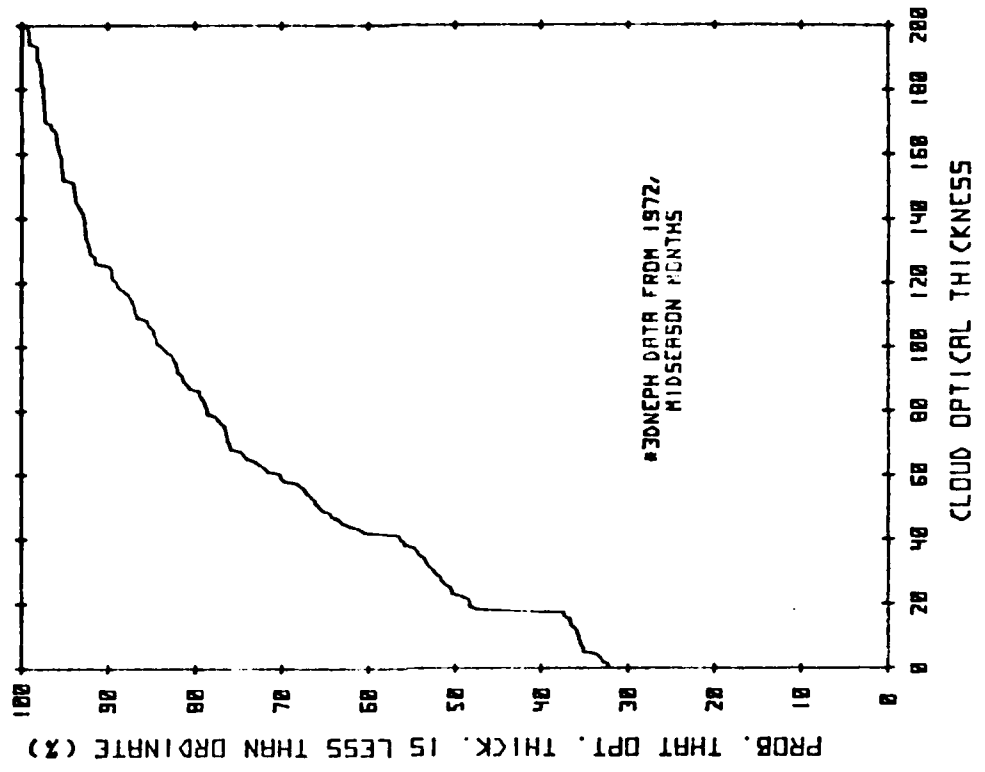


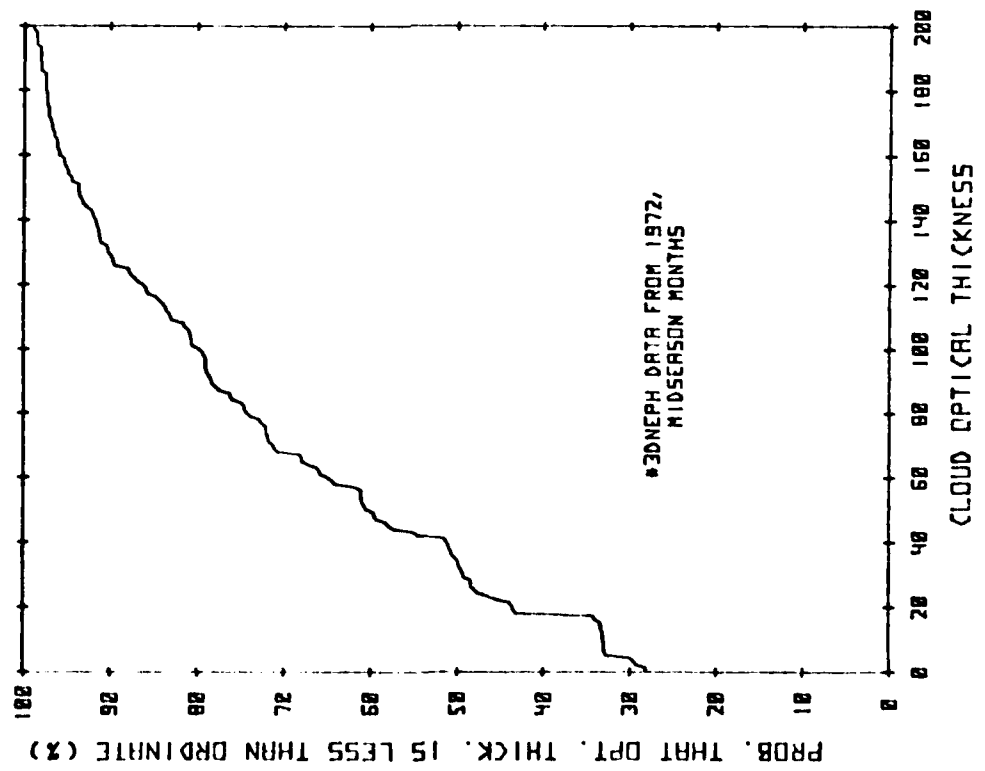
Figure 16

Figure 17

OPTICAL THICKNESS DISTRIBUTION FOR
LOCATION IN ATLANTIC
(LAT/LONG) = (60°N, 15°W)



OPTICAL THICKNESS DISTRIBUTION FOR
LOCATION IN ATLANTIC
(LAT/LONG) = (60°N, 30°W)



OPTICAL THICKNESS DISTRIBUTION FOR
LOCATION IN PACIFIC
(LAT, LONG) = (30°N, 165°E)

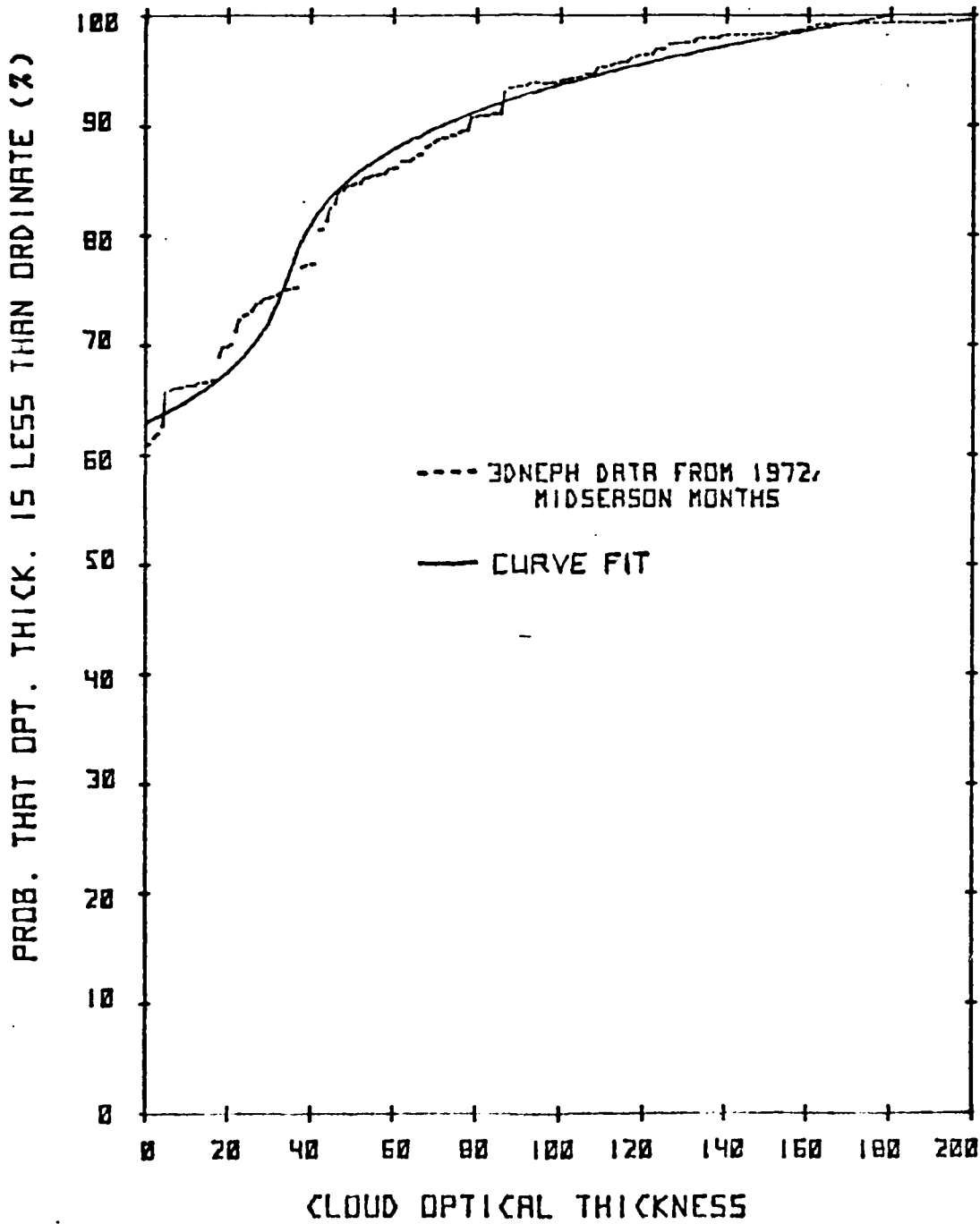


Figure 19

COEFFICIENTS FOR CURVE FITS TO
3DNEPH OPTICAL THICKNESS DISTRIBUTIONS

(Lat, Lon) N	f_0	a_0	a_1	a_2	a_3	a_4	a_5
(15., -130.) 3	.5657	.49021E+03	-.18676E+04	.20455E+04	-.46636E+03		
(25., -135.) 3	.6373	-.37311E+04	.14371E+05	-.18511E+05	.80773E+04		
(30., -150.) 3	.5356	-.14118E+04	.60584E+04	-.86365E+04	.41943E+04		
(40., -150.) 3	.3642	-.27997E+03	.13528E+04	-.20256E+04	.11585E+04		
(40., -165.)*	.3642	-.27997E+03	.13528E+04	-.20256E+04	.11585E+04		
(40., 180.) 3	.4056	-.53818E+03	.25015E+04	-.36658E+04	.18976E+04		
(50., -165.) 3	.3579	-.26036E+03	.12862E+04	-.19747E+04	.11554E+04		
(50., 180.) 3	.2880	-.14918E+03	.83092E+03	-.13347E+04	.86181E+03		
(60., 180.) 3	.2555	-.14056E+03	.88687E+03	-.15805E+04	.10275E+04		
(50., 165.) 3	.3307	-.22535E+03	.11649E+04	-.18307E+04	.11154E+04		
(20., 180.) 4	.6824	.68687E+05	-.34118E+06	.63241E+06	-.51867E+06	.15891E+06	
(30., 165.) 3	.5977	-.16514E+04	.64740E+04	-.85105E+04	.38507E+04		
(20., 165.) 3	.5524	-.19181E+04	.79777E+04	-.11011E+05	.51683E+04		
(20., 150.) 3	.6466	-.47331E+04	.18194E+05	-.23331E+05	.10074E+05		
(30., 150.) 3	.6086	-.27808E+04	.11047E+05	-.14629E+05	.65481E+04		
(30., 135.) 3	.5132	-.13905E+04	.58560E+04	-.8164E+04	.38489E+04		
(20., 120.)*	.6225	-.18391E+04	.76337E+04	-.10344E+05	.47497E+04		
(30., 120.) 3	.6823	-.45813E+04	.17336E+05	-.21975E+05	.93783E+04		
(30., 180.) 3	.6105	-.16028E+04	.65780E+04	-.90887E+04	.42822E+04		
(30., -165.) 3	.6302	-.41800E+04	.16364E+05	-.21300E+05	.92964E+04		
(40., 165.) 3	.4377	-.78225E+03	.35953E+04	-.53078E+04	.26959E+04		
(40., 150.) 3	.3907	-.26998E+03	.12451E+04	-.17960E+04	.10197E+04		
(40., 135.) 3	.4961	-.97806E+03	.41322E+04	-.57186E+04	.27478E+04		
(50., 150.) 3	.3516	-.28646E+03	.14238E+04	-.21651E+04	.12309E+04		
(50., 135.) 3	.3742	-.22408E+03	.10294E+04	-.14769E+04	.87207E+03		
(30., 75.)* 4	.7188	.51088E+05	-.25585E+06	.47749E+06	-.39378E+06	.12120E+06	
(30., 60.)* 4	.7188	.51088E+05	-.25585E+06	.47749E+06	-.39378E+06	.12120E+06	
(30., 45.)* 4	.7188	.51088E+05	-.25585E+06	.47749E+06	-.39378E+06	.12120E+06	
(30., 30.)* 4	.7188	.51088E+05	-.25585E+06	.47749E+06	-.39378E+06	.12120E+06	
(36., -15.)* 4	.7188	.51088E+05	-.25585E+06	.47749E+06	-.39378E+06	.12120E+06	
(39., 74.) 3	.4406	-.76731E+03	.38442E+04	-.63146E+04	.35003E+04		
(50., 60.) 3	.3723	-.38159E+03	.19986E+04	-.33274E+04	.19132E+04		
(40., 60.) 3	.3522	-.94651E+02	.39688E+03	-.51067E+03	.41702E+03		
(40., 45.) 3	.4710	-.56176E+03	.25021E+04	-.37045E+04	.19627E+04		
(50., 45.) 3	.2679	-.12116E+03	.70420E+03	-.11462E+04	.76809E+03		
(50., 30.) 3	.3257	-.14502E+03	.73016E+03	-.11120E+04	.72873E+03		
(40., 30.) 3	.4986	-.11924E+04	.53915E+04	-.80030E+04	.39833E+04		
(40., 15.) 3	.5611	-.16022E+04	.66000E+04	-.90262E+04	.41929E+04		
(50., 15.) 3	.3277	-.15279E+03	.75818E+03	-.11238E+04	.71074E+03		
(35., -30.)* 4	.7188	.51088E+05	-.25585E+06	.47749E+06	-.39378E+06	.12120E+06	
(60., 46.) 3	.3756	-.38635E+03	.20296E+04	-.34031E+04	.19765E+04		
(67., 26.) 3	.2339	-.94433E+02	.65444E+03	-.11787E+04	.84662E+03		
(60., 30.) 3	.2852	-.11326E+03	.62710E+03	-.10002E+04	.67947E+03		
(60., 15.) 3	.3206	-.19413E+03	.10649E+04	-.17907E+04	.11163E+04		
(70., 15.) 3	.4621	-.79140E+03	.36455E+04	-.54635E+04	.27713E+04		
(70., 0.) 3	.3549	-.20658E+03	.10509E+04	-.16587E+04	.95151E+03		
(60., 0.) 3	.2404	-.11791E+03	.75450E+03	-.13091E+04	.87669E+03		
(50., 0.)* 3	.3277	-.15279E+03	.75818E+03	-.11238E+04	.71074E+03		
(40., 0.) 5	.5106	-.23734E+05	.17225E+06	-.49405E+06	.69937E+06	-.48964E+06	.13543E+06

Latitude is in + degrees North
Longitude is in + degrees West

*3DNEPH data not yet obtained for these locations; Coefficients shown are for neighboring distributions, and represent best estimates until actual data is obtained.

THIS PAGE IS UNCLASSIFIED
DATE 10/10/01 BY 60322 UCBAW